Supplementary Information (SI) for Journal of Materials Chemistry A.
This journal is © The Royal Society of Chemistry 2026

Supporting Information

Sequential Surface Synthesis of Dispersed Sub-Nanometer Iridium on Titanium Nitride for Acidic Water Oxidation

Wenhao Liu[1,2], Zhenhua Xie[3], Lihua Zhang[1], Jingguang G. Chen[3],*

Fang Lu[1], Yugang Zhang[1*]*

[1]Center for Functional Nanomaterials, Energy & Photon Sciences Directorate, Brookhaven National Laboratory, Upton, NY 11973, USA.

[2]Department of Materials Science and Chemical Engineering, Stony Brook University, Stony Brook, New York11794, United State

[3]Chemistry Division, Brookhaven National Laboratory, Upton, New York 11973, United States

[4]Department of Chemical Engineering, Columbia University, New York, New York 10027, United States

*Corresponding authors

E-mails: flu@bnl.gov (https://orcid.org/0000-0003-3765-7615)
yuzhang@bnl.gov (https://orcid.org/0000-0002-7832-1475)
jgchen@columbia.edu (https://orcid.org/0000-0002-9592-2635)

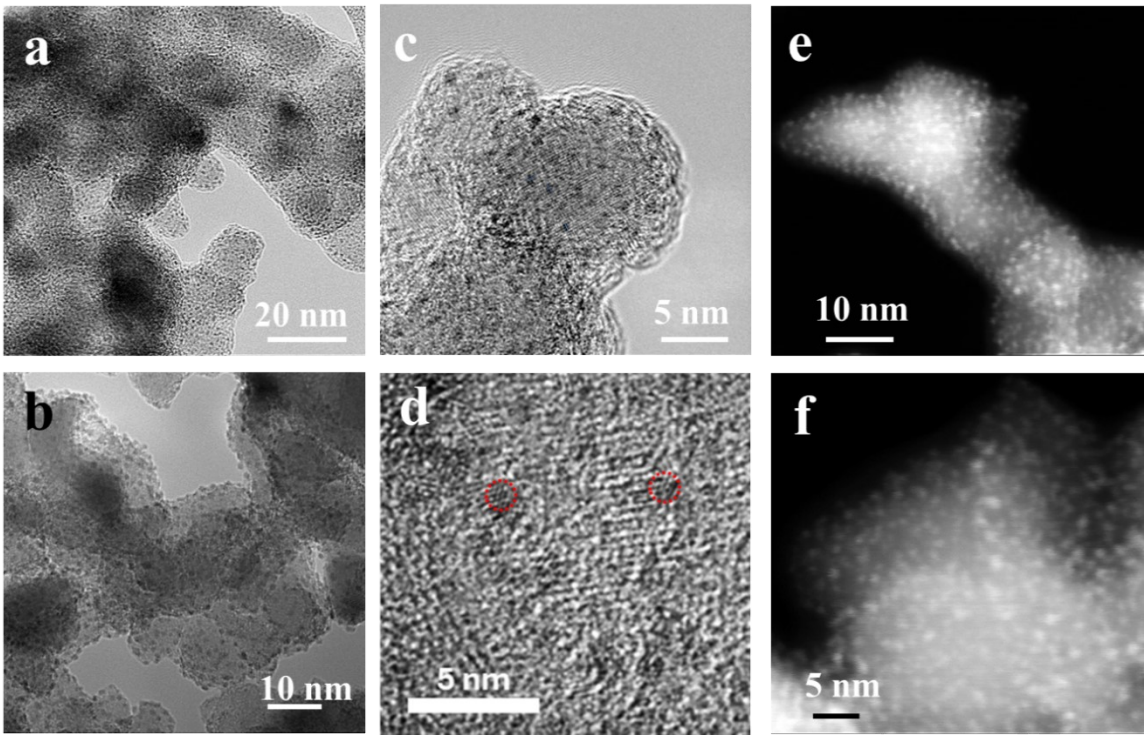

Figure S1. TEM images of as-synthesized Ir@TiN at various magnifications before thermal treatment.

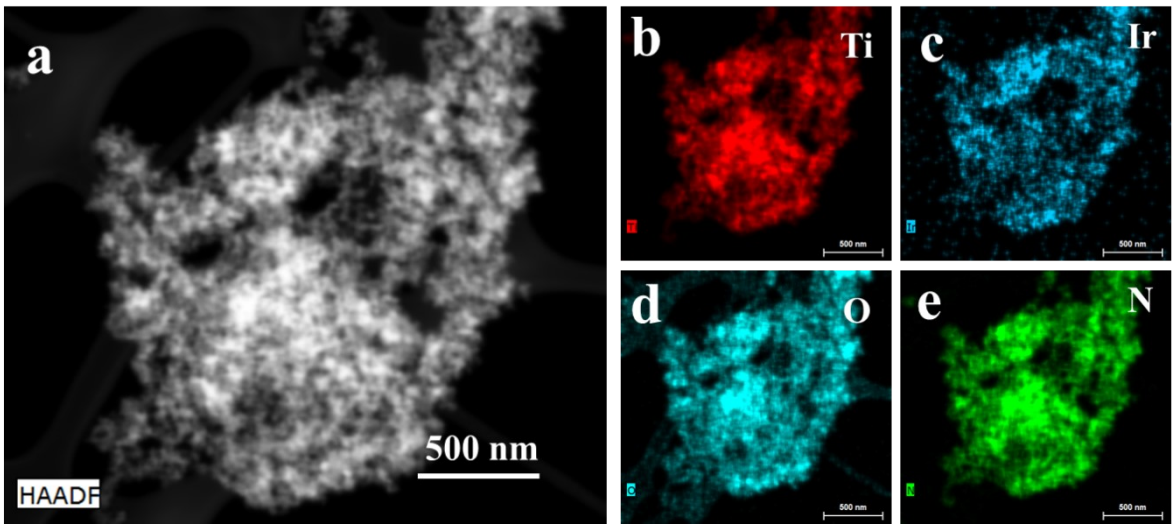

Figure S2. HAADF-STEM image and EDX elemental maps of as-synthesized Ir@TiN showing Ir, Ti, and N distribution.

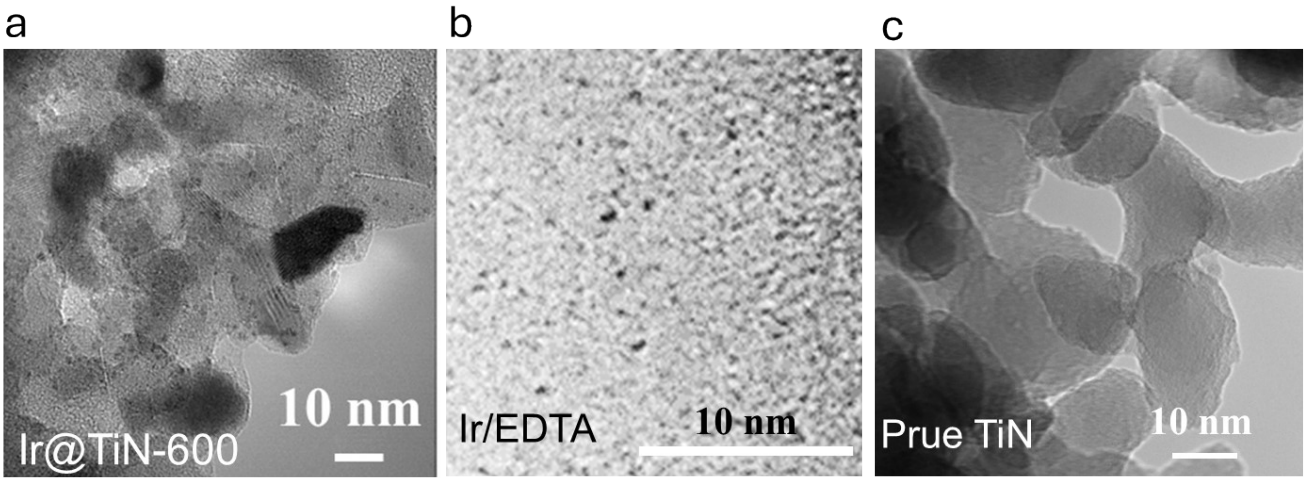

Figure S3. TEM images of (a) Ir@TiN-600 (annealed at 600°C) (b) Ir nanoparticles with EDTA, (c) Pure TiN.

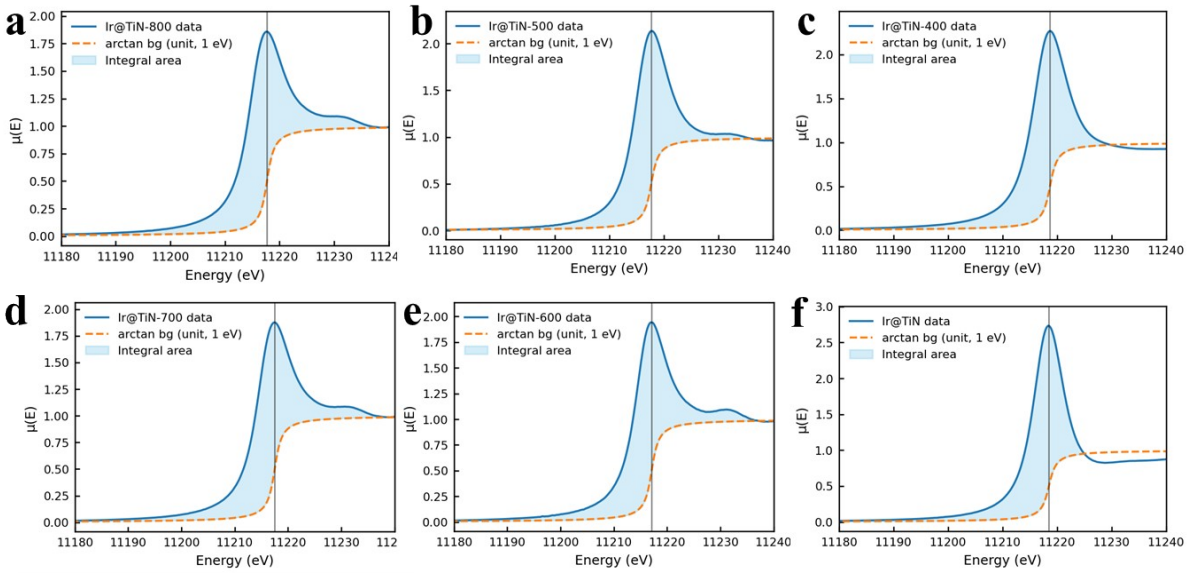

Figure S4. Ir L_3-edge XANES spectra with whiteline fitting for the thermal series. (A-F) Normalized spectra (blue) with arctangent background (orange). Shaded region indicates integrated whiteline area. Vertical lines mark whiteline maxima.

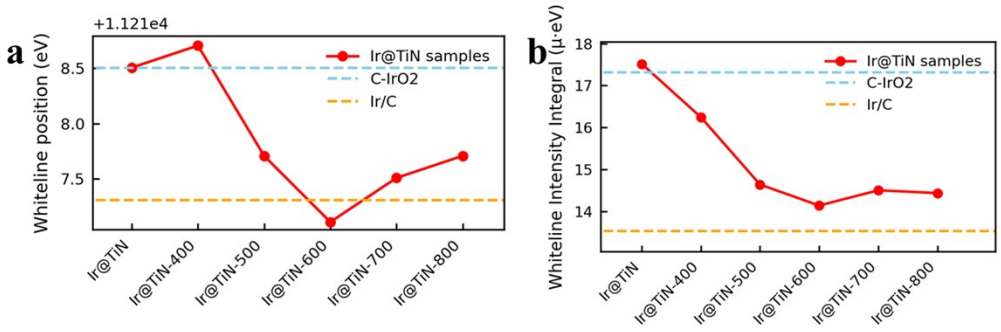

Figure S5. Whiteline metrics extracted from Figure S6. (a) Whiteline peak position versus annealing temperature. (b) Integrated whiteline intensity. Dashed lines indicate IrO_2 (oxidized) and Ir/C (metallic) references.

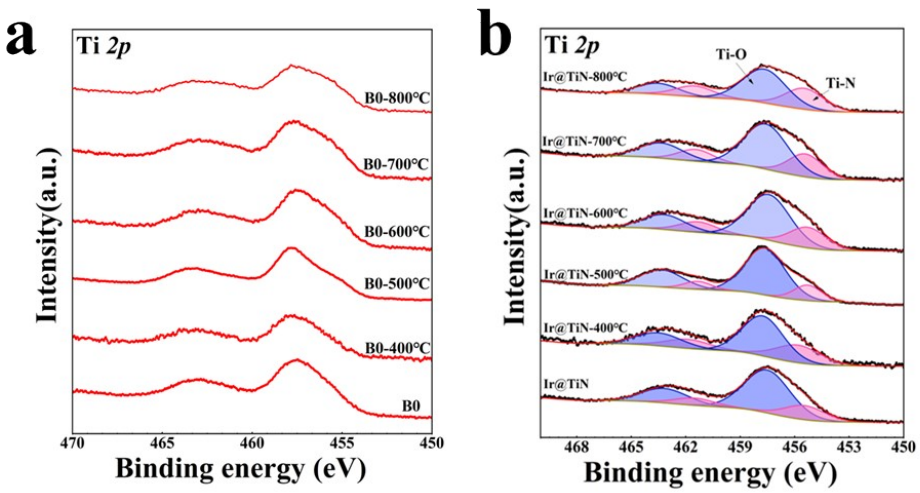

Figure S6. XPS Ti 2p spectra of the thermal series. (a) Raw spectra. (b) Fitted spectra showing Ti-N and Ti-O contributions.

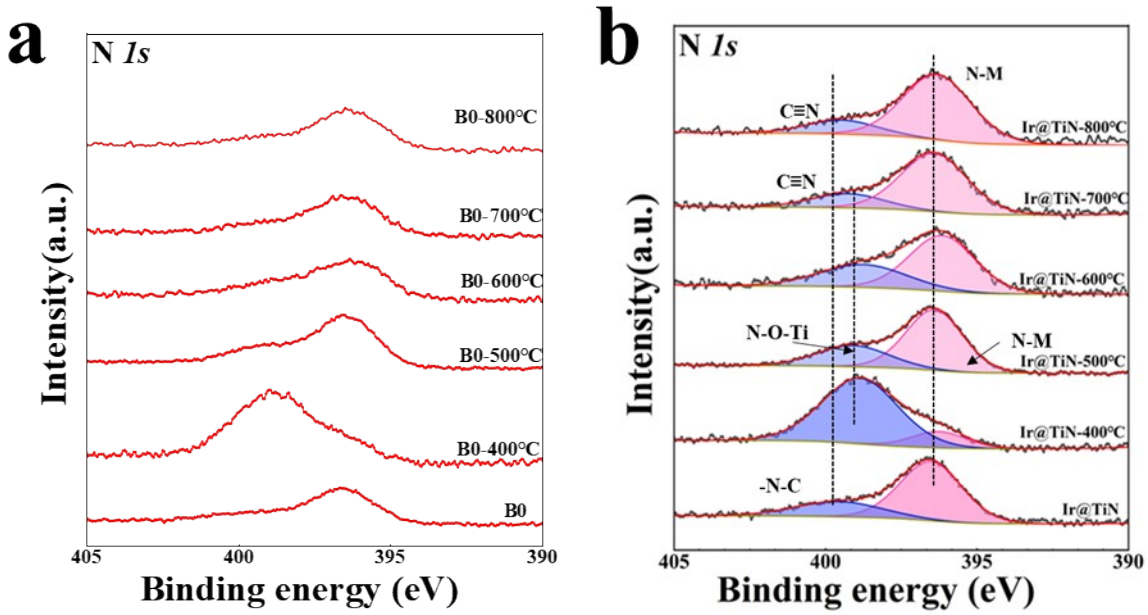

Figure S7. XPS N 1s spectra of the thermal series. (a) Raw spectra. (b) Fitted spectra.

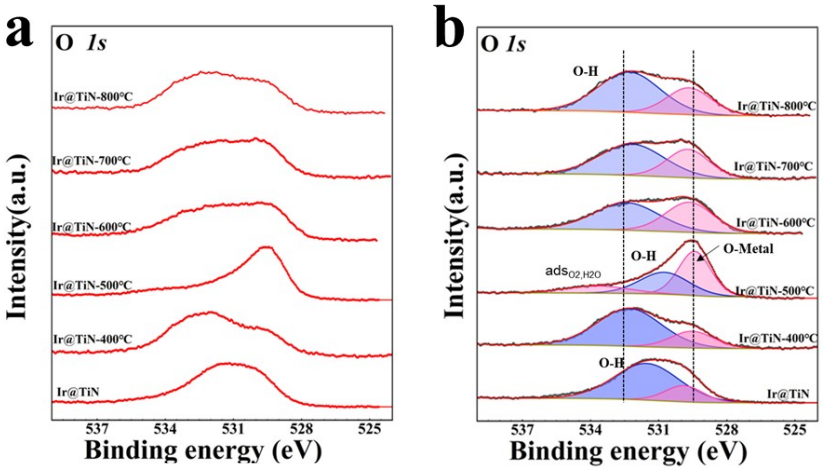

Figure S8. XPS O 1s spectra of the thermal series. (a) Raw spectra. (b) Fitted spectra.

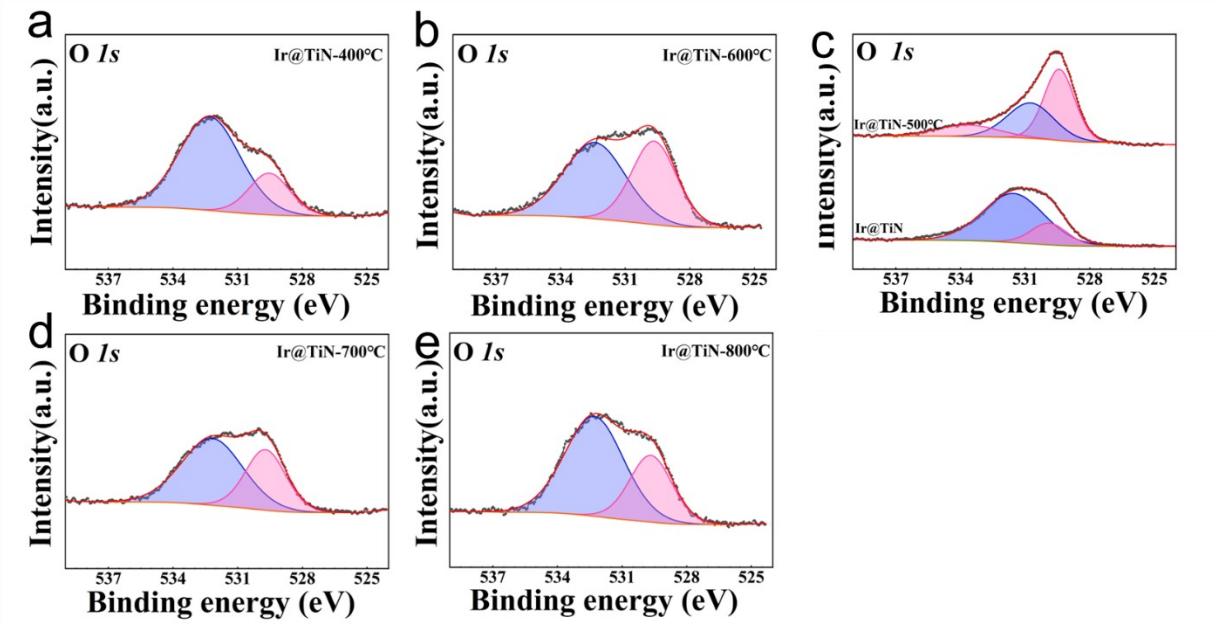

Figure S9. XPS spectra at different annealing temperatures. (a-d) O 1s spectra for Ir@TiN-400, -600, -700, and -800. (e) Raw Ir 4f spectra for all samples.

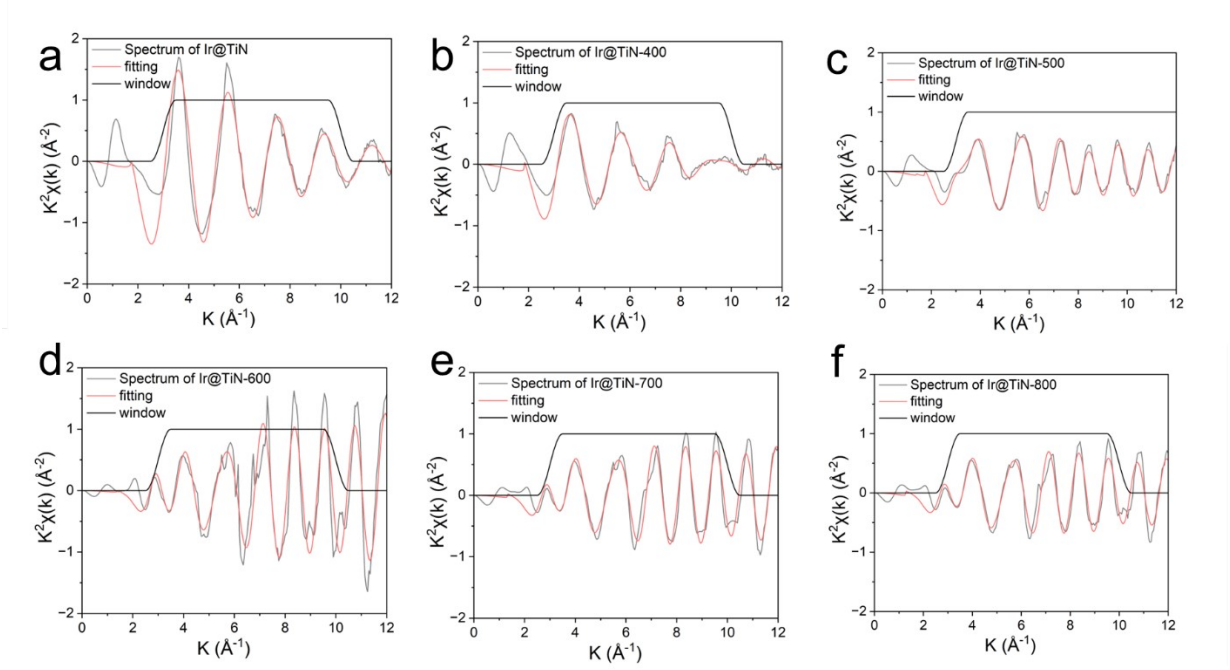

Figure S10. EXAFS spectra in k-space with fitting results for the thermal series.

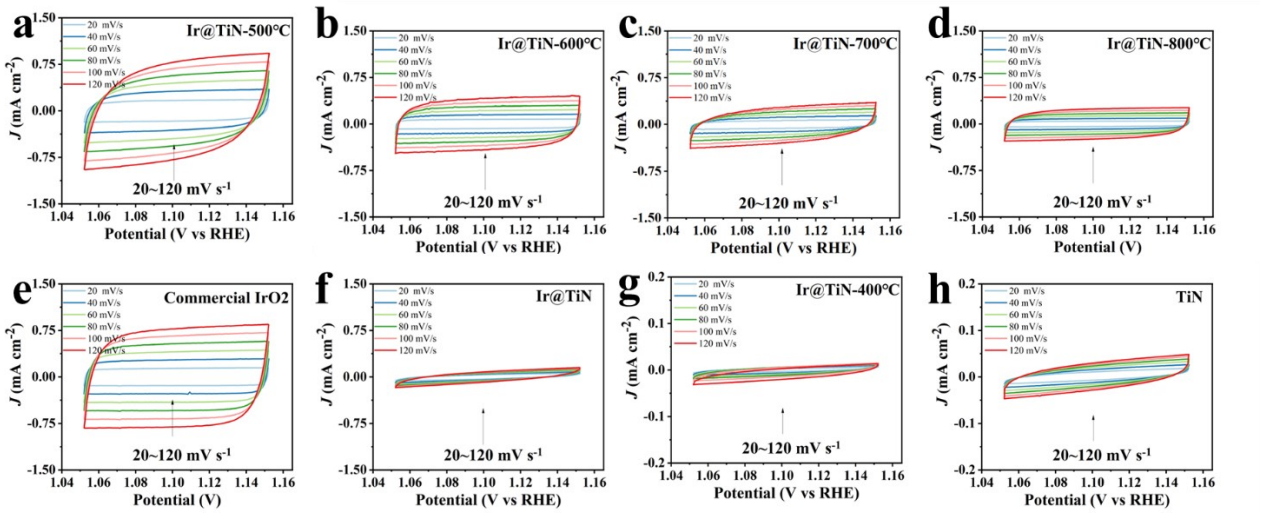

Figure S11. Cyclic voltammetry curves at scan rates from 20 to 120 mV s^{-1} for double-layer capacitance determination. (a) Ir@TiN-500. (b) Ir@TiN-600. (c) Ir@TiN-700. (d) Ir@TiN-800. (e) Commercial IrO_2. (f) As-synthesized Ir@TiN. (g) Ir@TiN-400. (h) TiN support.

The electrochemical active surface area (ECSA) was calculated from the electrochemical double-layer capacitance (C_{dl}) using equation:

$$ECSA = \frac{C_{dl}}{C_s}$$

where C_{dl} was measured by recording CV curves at different scan rates (20, 40, 60, 80,100,120 mV s^{-1}). In this work, a C_s value of 60 μF cm^{-2} was used to determine the ECSA as reported previously[1]. So ECSA value is (a) Ir@TiN-500 102.67 cm^2. (b) Ir@TiN-600 56.00 cm^2. (c) Ir@TiN-700 36.67 cm^2. (d) Ir@TiN-800 33.00 cm^2. (e) Commercial IrO_2 109.33 cm^2. (f) As-synthesized Ir@TiN 7.83 cm^2. (g) Ir@TiN-400 3.17 cm^2.

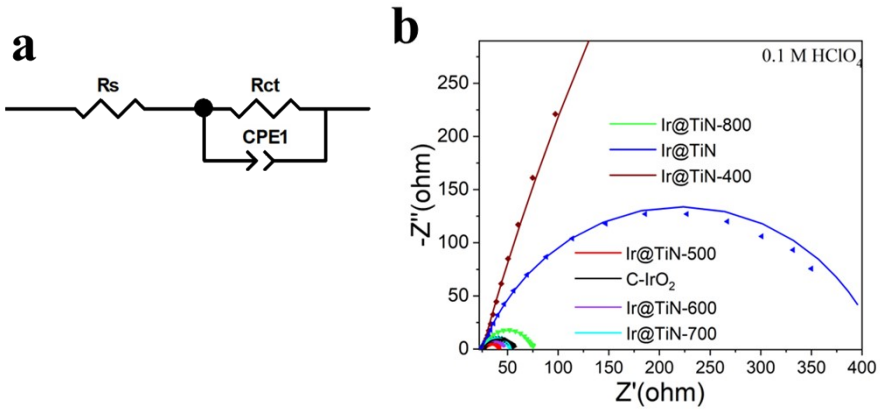

Figure S12. Electrochemical impedance spectroscopy analysis. (a) Equivalent circuit used for fitting. (b) EIS Nyquist plots for all samples.

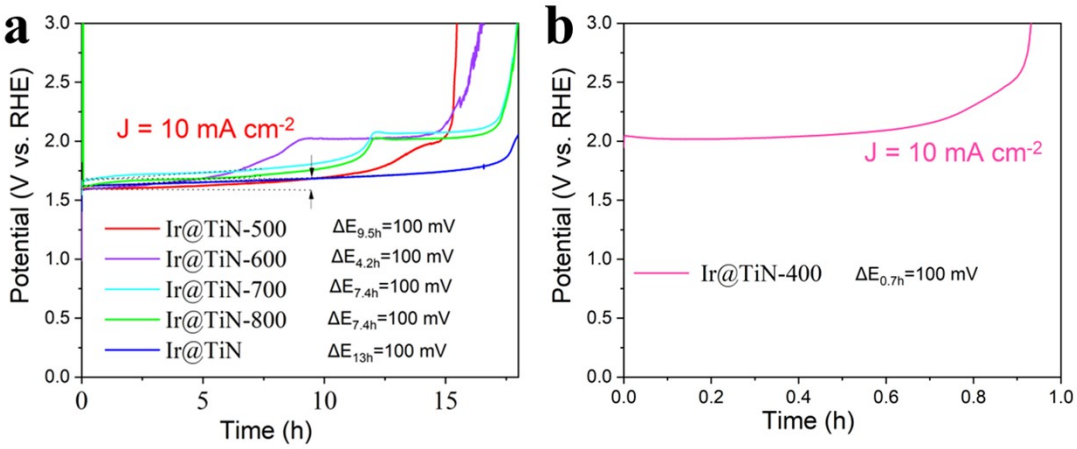

Fig.

Figure S13. Chronopotentiometry stability tests at 10 mA cm^{-2}. (a) Stability curves for the thermal series. (b) Expanded view of Ir@TiN-400.

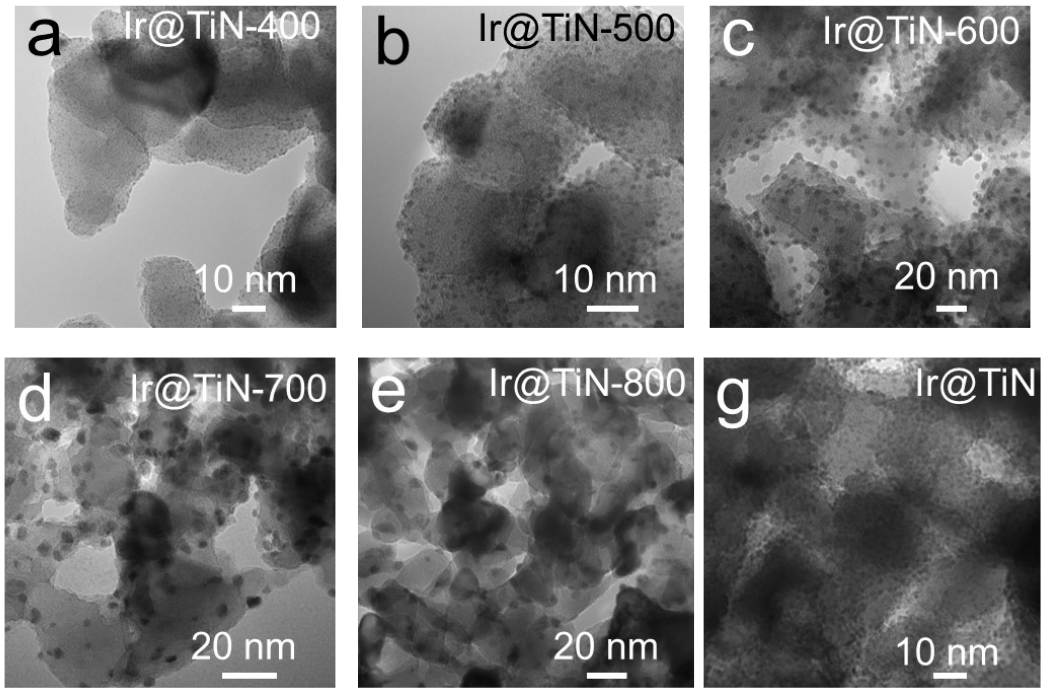

Figure S14. TEM images after stability testing. (a) Ir@TiN-400. (b) Ir@TiN-500. (c) Ir@TiN-600. (d) Ir@TiN-700. (e) Ir@TiN-800. (f) As-synthesized Ir@TiN.

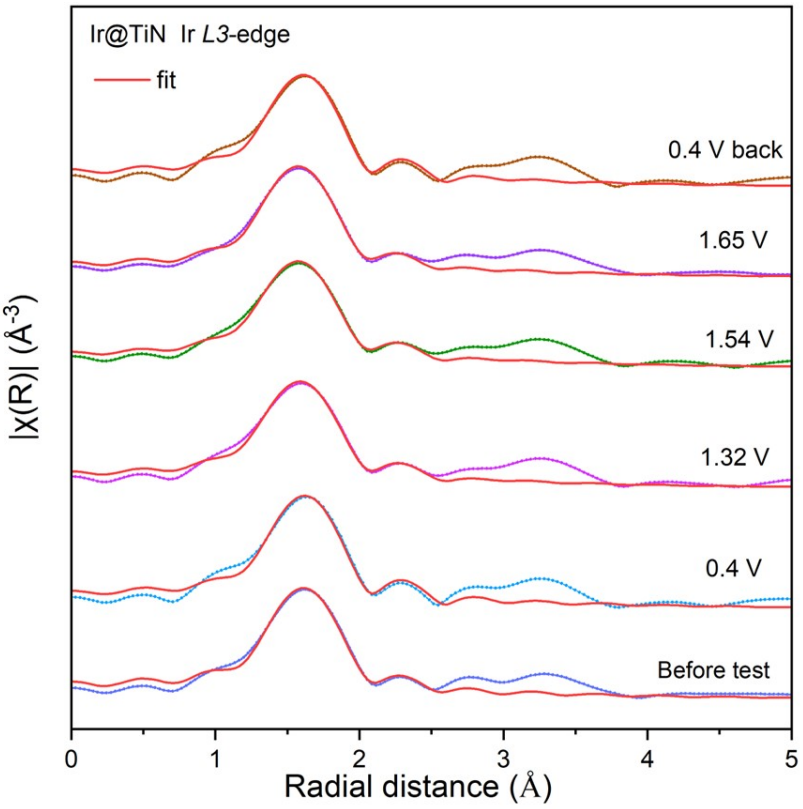

Figure S15. Fourier-transformed EXAFS spectra with fitting for Ir@TiN-500 at different applied potentials during operando measurements.

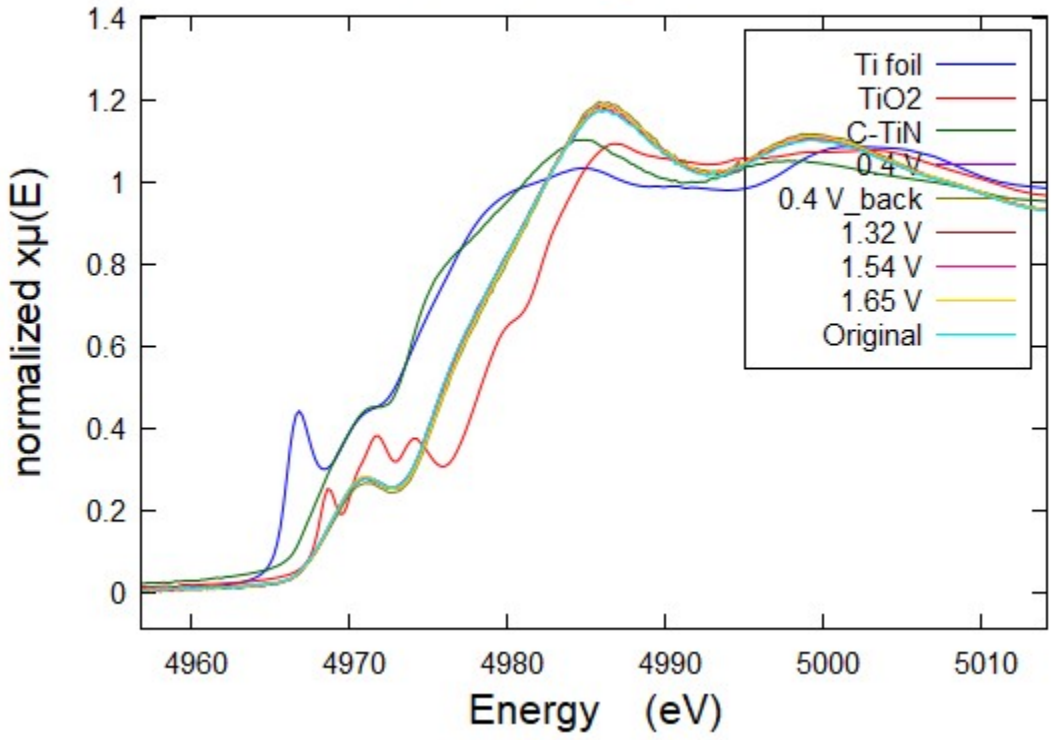

Figure S16. Operando XANES spectra at the Ti K-edge for Ir@TiN-500 at different potentials.

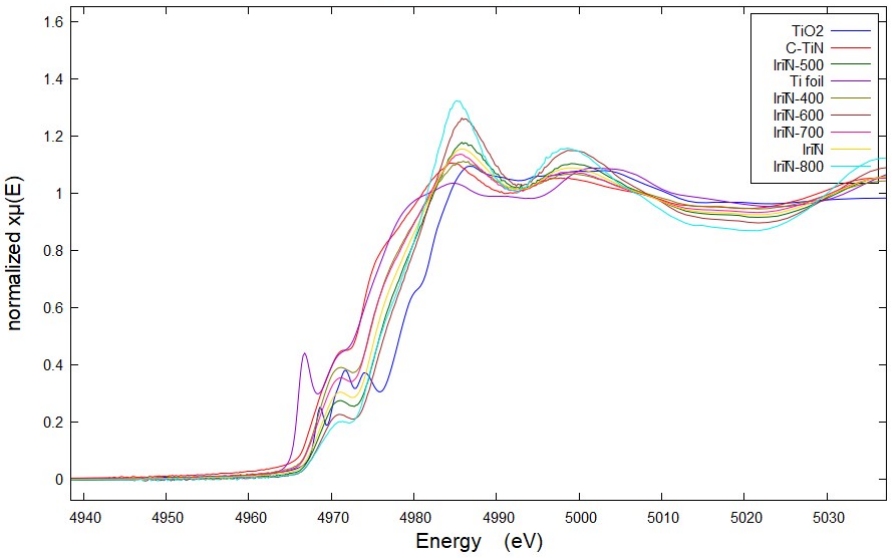

Figure S17. XANES spectra at the Ti K-edge for the thermal series.

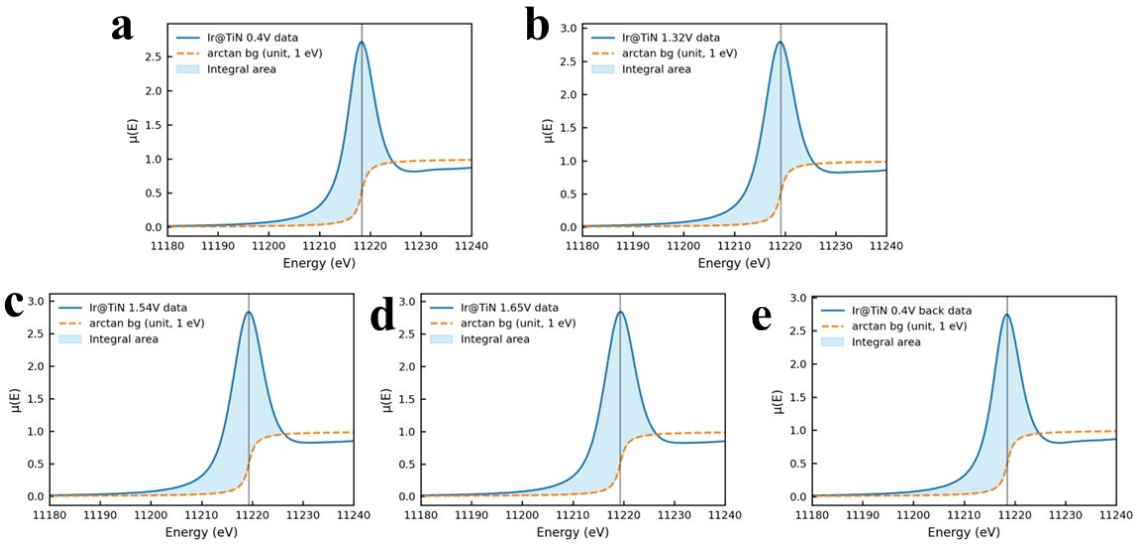

Figure S18. Operando Ir L_3-edge XANES with whiteline fitting for as-synthesized Ir@TiN. (a-e) Normalized spectra at 0.4 V, 1.32 V, 1.54 V, 1.65 V, and 0.4 V return. Dashed lines show arctangent background. Shaded regions indicate integrated whiteline area.

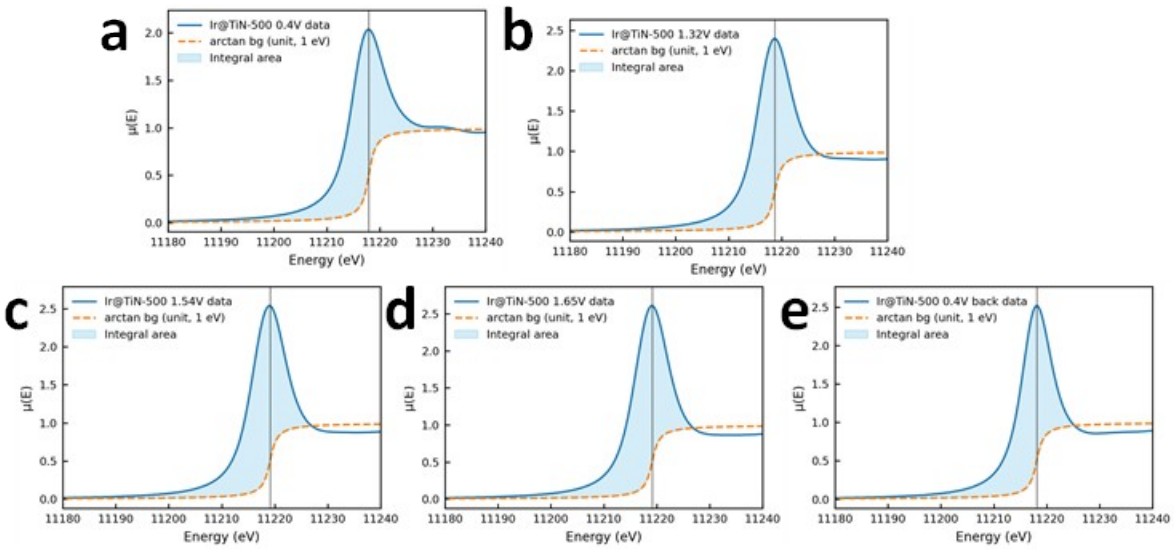

Figure S19. Operando Ir L_3-edge XANES with whiteline fitting for Ir@TiN-500. (a-e) Normalized spectra at 0.4 V, 1.32 V, 1.54 V, 1.65 V, and 0.4 V return.

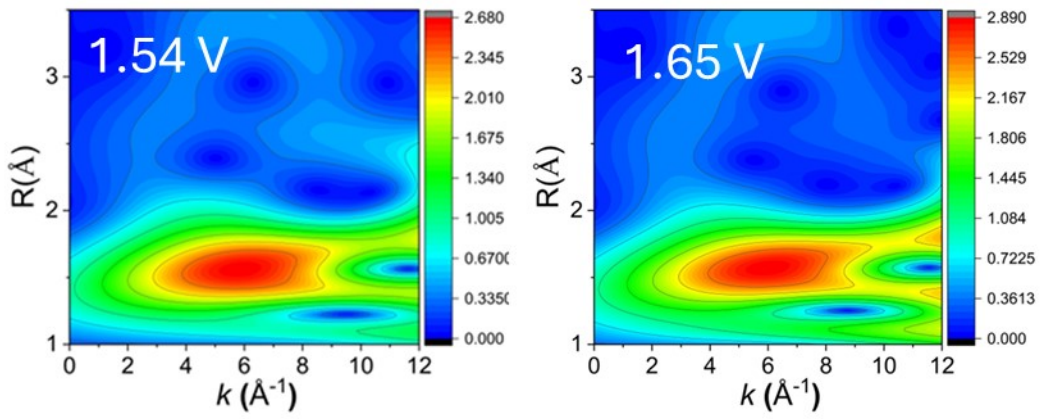

Figure S20 Wavelet transform analysis for samples of Ir@TiN-500 at 1.54V and 1.65V.

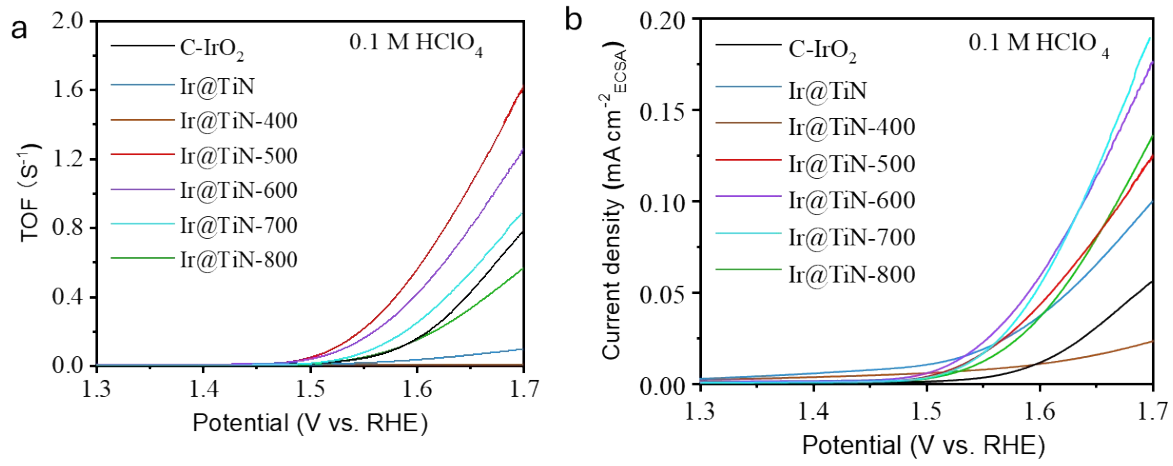

Figure S21. (a) TOF (b)Current density electrochemically active surface area (ECSA) (b).

Turnover frequency (TOF) values of the catalysts were calculated from the equation[2]:

$$TOF = \frac{j * A}{4 * F * n}$$

where j is the current density at a given potential, A is the surface area of the electrode, F is the Faraday constant (a value of 96485.3 C mol-1), and n is the amount of all Ir species on the electrode. All Ir atoms were assumed accessible for catalyzing OER.

Table S1. Electrochemical impedance parameters for Ir@TiN samples. Solution resistance (Rs) and charge-transfer resistance (Rct) obtained from EIS fitting.

Samples	Rs (Ω)	Rct (Ω)
B0_500℃	24.93	19.24
B0_600℃	24.43	25.74
B0_700℃	25.06	28.69
Commercial IrO2	25.58	32.82
B0_800℃	24.49	51.74
B0_400℃	25.23	4368
B0	24.57	385.2

Table S2. Chronopotentiometry stability at 10 mA cm^{-2}. Time required to reach 100 mV potential increase for each sample.

Samples	Ir@TiN	Ir@TiN-400	Ir@TiN-500	Ir@TiN-600	Ir@TiN-700	Ir@TiN-800
Time for 100 mV	13 h	0.7 h	9.5 h	4.2 h	7.4 h	7.4 h

Table S3. Electrochemical performance metrics for Ir@TiN samples and controls. Mass activity at 1.54 V vs. RHE, overpotential at 10 mA cm^{-2}, double-layer capacitance, and Tafel slope.

Sample	Mass activity (A/g_{Ir}) @1.54V	Potential at 10 mA/cm^2 (mV)	Capacitance (mF/cm^2)	Slope (mV/dec)
Ir@TiN	33		0.47	96.39
Ir@TiN-400	10		0.19	182.8
Ir@TiN-500	342	325	6.16	39.47
Ir@TiN-600	255	340	3.36	44.76
Ir@TiN-700	118	369	2.2	46.44
Ir@TiN-800	79	399	1.98	54.38
C_IrO2	76	390	6.56	44.78
TiN			0.08	

Table S4. XPS Ir 4f peak positions and assignments for the thermal series. Binding energies relative to Ir@TiN-500 (reference: 61.6 eV for Ir $4f_{7/2}$).

Samples	Peak1 (eV)				Peak2 (eV)			
	$4f_{5/2}$		$4f_{7/2}$		$4f_{5/2}$		$4f_{7/2}$	
Ir@TiN	64.95	+0.25	61.85	+0.25				
	Ir-O		Ir-O					
Ir@TiN-400	65.25	+0.55	62.15	+0.55				
	Ir-O		Ir-O					
Ir@TiN-500	64.7	0	61.6	0	63.65	0	60.9	0
	Ir-O		Ir-O		Ir-Ir		Ir-Ir	
Ir@TiN-600	65.75	+1.05	62.4	+0.8	63.8	+0.15	60.7	-0.2
	Ir-O		Ir-O		Ir-Ir		Ir-Ir	
Ir@TiN-700					64.00	+0.35	60.9	0
					Ir-Ir		Ir-Ir	
Ir@TiN-800					63.7	+0.05	60.6	-0.3
					Ir-Ir		Ir-Ir	

Table S5. XPS Ti 2p peak positions and assignments for the thermal series.

Samples	Peak1 (eV)				Peak2 (eV)			
	$2p_{3/2}$		$2p_{1/2}$		$2p_{3/2}$		$2p_{1/2}$	
Ir@TiN	463	-0.05	458	-0.05	462	0.35	456	0.3
Ir@TiN-400	464	0.25	458	0.1	462	0.75	456	0.7
Ir@TiN-500	463	0	458	0	461	0	455	0
Ir@TiN-600	463	-0.05	458	-0.15	461	0.05	455	0.05
Ir@TiN-700	464	0.1	458	0	462	0.15	456	0.15
Ir@TiN-800	464	0.25	458	0.1	462	0.25	456	0.25
bonds	Ti-O				Ti-N			

Table S6. XPS N 1s peak positions and assignments for the thermal series.

Table S5. XPS Peak Positions of N *1s* for Ir@TiN Samples at Different Temperatures. **Samples**	**Peak1 (eV)**	**Peak2 (eV)**
Ir@TiN	399.65	396.55
	-N-C	N-Metal
Ir@TiN-400	398.9	396.3
	N-O-Ti	N-Metal
Ir@TiN-500	399.15	396.45
	N-O-Ti	N-Metal
Ir@TiN-600	398.8	396.2
	N-O-Ti	N-Metal
Ir@TiN-700	399.3	396.45
	C≡N	N-Metal
Ir@TiN-800	399.55	396.4
	C≡N	N-Metal

Table S7. XPS O 1s peak positions and assignments for the thermal series.

Samples	Peak1 (eV)		Peak2 (eV)	
Ir@TiN	531.6	+0.80	529.95	+0.50
	O-H		**O-Metal**	
Ir@TiN-400	532.35	+1.55	529.55	+0.10
	O-H		**O-Metal**	
Ir@TiN-500	530.8	0	529.45	0
	533.75 ($adsO_2$, H_2O)	O-H	**O-Metal**	
Ir@TiN-600	532.45	+1.65	529.7	+0.25
	O-H		**O-Metal**	
Ir@TiN-700	532.25	+1.45	529.75	+0.30
	O-H		**O-Metal**	
Ir@TiN-800	532.35	+1.55	529.7	+0.25
	O-H		**O-Metal**	

Table S8. EXAFS fitting results for the thermal series. Coordination numbers (CN), bond lengths, Debye-Waller factors (σ^2), and energy shifts (E_0) for Ir-Ir and Ir-O shells.

Potentials	Shell	CN	Bond length	σ^2 (Å^2)	E0	R
B0	Ir-Ir(Ti)	0.21±0.94	2.48±0.25	0.0040	11.38	0.014
	Ir-O(N)	6.38±1.12	2.03±0.015	0.0040	11.38	
400	Ir-Ir(Ti)	1.79±1.27	2.54±0.08	0.0038	12.18	0.011
	Ir-O(N)	4.58±0.91	2.03±0.01	0.0038	12.18	
500	Ir-Ir	5.32±0.5	2.68±0.01	0.0055	7.14	0.005
	Ir-O(N)	2.34±0.3	2.01±0.01	0.0055	11.70	
600	Ir-Ir	9.84±1.6	2.70±0.009	0.0034	7.57	0.008
	Ir-O(N)	0.54±0.31	2.00±0.049	0.0034	7.57	
700	Ir-Ir	8.86±0.93	2.70±0.006	0.0048	6.63	0.003
	Ir-O(N)	0.72±0.17	1.96±0.021	0.0048	6.63	
800	Ir-Ir	8.78±1.1	2.72±0.008	0.0059	6.24	0.005
	Ir-O(N)	0.82±0.2	2.01±0.023	0.0059	6.24	

Table S9. Operando EXAFS fitting results for Ir@TiN-500 at different applied potentials.

Potentials	Shell	CN	Bond length	σ^2 ($Å^2$)	E0	R
Before	Ir-Ir	5.32±0.5	2.68±0.01	0.0055	7.14	0.005
	Ir-O	2.34±0.3	2.01±0.01	0.0055	11.70	
OCP	Ir-Ir	4.95±0.5	2.68±0.01	0.0052	7.75	0.010
	Ir-O	2.58±0.4	2.01±0.002	0.0079	11.14	
0.4V	Ir-Ir	4.62±0.5	2.68±0.01	0.0056	7.32	0.008
	Ir-O	2.41±0.3	2.01±0.002	0.0068	9.34	
1.32V	Ir-Ir	1.96±1.2	2.65±0.01	0.0064	4.02	0.020
	Ir-O	4.21±0.6	1.98±0.002	0.0059	9.09	
1.54V	Ir-Ir	0.68±0.9	2.68±0.090	0.0059	9.09	0.021
	Ir-O	5.09±0.9	1.97±0.017			
1.65V						0.024
	Ir-O	5.87±0.5	1.97±0.001	0.0058	10.98	
0.4V-back	Ir-Ir	0.34±0.9	2.62±0.04	0.0047	11.17	0.019
	Ir-O	5.17±1.2	2.02±0.01	0.0047	11.17	

Table S10. Operando EXAFS fitting results for as-synthesized Ir@TiN at different applied potentials.

Potentials	**Shell**	**CN**	**Bond length**	**σ^2 (Å^2)**	**E0**	**R**
Before	Ir-Ir	0.21±0.94	2.48±0.25	0.0040	11.38	0.014
	Ir-O(N)	6.38±1.12	2.03±0.015	0.0040	11.38	
0.4V	Ir-Ir	0.94±1.24	2.48±0.069	0.0030	11.66	0.016
	Ir-O(N)	7.07±1.27	2.04±0.017	0.0030	11.66	
1.32 V	Ir-Ir	0.83±1.12	2.48±0.085	0.0063	11.87	0.013
	Ir-O(N)	7.09±1.19	2.00±0.016	0.0063	11.82	
1.54 V	Ir-Ir	0.85±1.29	2.49±0.087	0.0066	11.38	0.015
	Ir-O(N)	7.11±1.32	1.98±0.017	0.0066	12.34	
1.65 V	Ir-Ir	0.89±01.34	2.48±0.25	0.0064	11.80	0.016
	Ir-O(N)	7.01±1.36	1.98±0.013	0.0064	11.80	
0.4V back	Ir-Ir	0.97±1.14	2.51±0.065	0.0051	11.67	0.016
	Ir-O(N)	7.08±1.21	2.03±0.015	0.0051	11.67	

Table S11. OER performance of Ir-based electrocatalysts in acidic medium.

Catalyst	Electrolyte	Overpotential (mV) @10 mA cm^{-2}	Mass activity (A g_{Ir}^{-1})	Stability (h) @ 10 mA cm^{-2}	Reference
Commercial IrO_2	0.1 M $HClO_4$	390	76 @1.54V	-	This work
Ir@TiN-500	**0.1 M $HClO_4$**	**325**	**342 @1.54V**	**9.5**	**This work**
IrO2@Ir/TiN	0.5 M $H2SO_4$	265	480.4 @ 1.6 V	6	[2]
TiN/IrO2	0.5 M $H2SO_4$	313	874 @ 1.6 V	<2.3	[3]
IrFeCoNiCu-HEA	0.1 M $HClO_4$	302	34.67 @1.53V	12	[4]
Ir-doped MnO2	0.5 M $H2SO_4$	218	766@1.53V	650	[5]
Mn0.8Ir0.2Oy	0.5 M $H2SO_4$	300	~294@1.53V	-	[6]
Ir NS/TiO_2	0.05 M H_2SO_4	-	363 @1.55V	100	[7]
Ir-$LiCoO_2$	0.5 M $H2SO_4$	≈233	433 @ 1.51V	1200	[8]
Ir/$WO_{2.72}$/TF	0.5 m H_2SO_4	259	1202.5 @1.53V	150	[9]
Ir_1O_6–Co_3O_4	0.1 M $HClO_4$	253	519 @ 1.53V	200	[10]
CO-IrO_x/oxi-TiN	0.1 M $HClO_4$	277	542 @ 1.54V	100	[1]
IrO_x/ TiN	0.1 M $HClO_4$	293	270.8 @ 1.54V	250	[11]

Reference:

(1) Han, X.; Mou, T.; Kang, S.; Islam, A.; Zhao, X.; Sasaki, K.; Rodriguez, J. A.; Chang, Q.; Liu, P.; Chen, J. G. Enhancing Acidic Oxygen Evolution Activity by Controlling Oxidation State of Iridium. *Angew Chem Int Ed Engl* **2025**, *64* (33), e202507468.

(2) Li, G.; Li, K.; Yang, L.; Chang, J.; Ma, R.; Wu, Z.; Ge, J.; Liu, C.; Xing, W. Boosted Performance of Ir Species by Employing TiN as the Support toward Oxygen Evolution Reaction. *ACS Appl Mater Interfaces* **2018**, *10* (44), 38117-38124.

(3) Zhang, K. K.; Mai, W. S.; Li, J.; Wang, H.; Li, G. Q.; Hu, W. Highly scattered Ir oxides on TiN as an efficient oxygen evolution reaction electrocatalyst in acidic media. *Journal of Materials Science* **2020**, *55* (8), 3507-3520.

(4) Maulana, A. L.; Chen, P. C.; Shi, Z.; Yang, Y.; Lizandara-Pueyo, C.; Seeler, F.; Abruna, H. D.; Muller, D.; Schierle-Arndt, K.; Yang, P. Understanding the Structural Evolution of IrFeCoNiCu High-Entropy Alloy Nanoparticles under the Acidic Oxygen Evolution Reaction. *Nano Lett* **2023**, *23* (14), 6637-6644.

(5) Shi, Z. P.; Wang, Y.; Li, J.; Wang, X.; Wang, Y. B.; Li, Y.; Xu, W. L.; Jiang, Z.; Liu, C. P.; Xing, W.; et al. Confined Ir single sites with triggered lattice oxygen redox: Toward boosted and sustained water oxidation catalysis. *Joule* **2021**, *5* (8), 2164-2176.

(6) Ren, Z.; Wang, Y.; Jiang, H.; Jiang, H.; Tian, M.; Liu, Y.; Han, J.; Fang, H.; Zhu, Y. A novel bifunctional catalyst for overall water electrolysis: nano Ir x Mn (1− x) O y hybrids with L1 2-IrMn 3 phase. *Chemical Communications* **2022**, *58* (5), 685-688.

(7) Shin, D.; Lee, S. J.; Bak, J.; Roh, J.; Lee, K.; Chang, H.; Lee, H.; Kim, M.; Yang, H. J.; Kim, S.; et al. Ultrathin Iridium Nanosheets on Titanium Oxide for High-Efficiency and Durable Proton Exchange Membrane Water Electrolysis. *ACS Nano* **2025**, *19* (50), 42556-42565.

(8) Liu, Y.; Jang, H.; Xi, X. K.; Zhong, Y.; Cao, R. G.; Jiao, S. H.; Li, X. Y.; Lei, Z. W.; Luo, J.-. Strong Catalyst-Support Interaction Stabilizes IrOx Nanoclusters for Efficient Acidic Oxygen Evolution. *Advanced Functional Materials* **2025**, *n/a* (n/a), e15920.

(9) Wang, W. J.; Zhang, Z.; Chu, B. X.; Peng, J. W.; Li, N.; Li, L.; Gu, M. D.; Xiao, X.; Xu, Q. Subnanometric Iridium Clusters Atomically Enrooted on Non-Stoichiometric Tungsten Oxides for Boosting Acidic Oxygen Evolution Reaction. *Advanced Functional Materials* **2025**, *n/a* (n/a), e20812.

(10) Li, W.; Zhang, J.; Yang, C.; Geng, Z.; Chen, X.; Liu, Q.; Wang, B.; Wang, L. Modulating Iridium Coordination to Control the Oxygen Evolution Reaction Pathway. *J Am Chem Soc* **2025**, *147* (44), 40697-40707.

(11) Han, X.; Mou, T.; Islam, A.; Kang, S.; Chang, Q.; Xie, Z.; Zhao, X.; Sasaki, K.; Rodriguez, J. A.; Liu, P.; et al. Theoretical Prediction and Experimental Verification of IrO(x) Supported on Titanium Nitride for Acidic Oxygen Evolution Reaction. *J Am Chem Soc* **2024**, *146* (24), 16499-16510.